IET Image Processing

Research Article

IET Journals
The Institution of Engineering and Technology

Fourier transform-based windowed adaptive switching minimum filter for reducing periodic noise from digital images

ISSN 1751-9659
Received on 1st December 2015
Revised on 8th February 2016
Accepted on 25th March 2016
doi: 10.1049/iet-ipr.2015.0750
www.ietdl.org

Justin Varghese[1] ✉, *Saudia Subash*[2], *Nasser Tairan*[1]

[1]*Department of Computer Science, King Khalid University, Gregar, Abha, Asir 61411, KSA*
[2]*Centre for Information Technology and Engineering, Manonmaniam Sundaranar University, Tirunelveli, Tamilnadu 627012, India*
✉ *E-mail: justin_var@yahoo.com*

Abstract: This paper presents a windowed adaptive switching minimum filter in frequency domain to restore images corrupted by periodic noise. Periodic noise frequencies that spread throughout the spatial domain image concentrate in frequency domain image as star-shaped peak regions. The proposed algorithm incorporates distinct stages of noisy frequency detection and correction. The noisy frequency detection stage has peak detection and noise map generation sub-stages to effectively identify noisy peak areas into a binary flag image from the directional image of the origin shifted Fourier transformed corrupted image. The proposed noise correction scheme restores the detected noisy areas of the corrupted frequency domain image with the minimum of nearest possible uncorrupted frequencies. Finally, inverse shifting and inverse Fourier transform operations generates the restored image. Experimental results in terms of subjective and objective metrics demarcate that the proposed periodic noise reduction filter is more effective in restoring images corrupted with periodic noise than other filters used in the comparative study.

1 Introduction

Periodic/quasi-periodic noises are repetitive noise patterns that affect digital images during image acquisition stage due to thermal/electrical/electro-mechanical interferences [1]. The noise also affects digital images when acquired by imaging systems mounted on vibrating holders such as helicopters, aircrafts, satellites and moving platforms [2]. These periodic noise degradations are very common in all imaging processes including medical [3], remote sensing and television transmission [4]. Hence, the restoration of periodic noise corrupted images is an important task in digital image processing [5]. Periodic noises are classified as global, local and stripping periodic noises [6]. The Global periodic noise affects the entire image with fixed parameters during transmission/acquisition stages due to the interference of independent signal sources. Local periodic noise affects a portion of image pixels during acquisition with varying parameters that depends on the sensed area. Stripping noise occurs due to the errors in sensor arrays and it disturbs the pixels of periodic row/column of the sensed image. The quasi-periodic noise affects all areas of digital image and so necessitates the correction of noisy peaks and its neighbouring spectral frequencies in frequency domain [7]. These periodic/quasi-periodic noises are predictable only in the frequency domain since noisy frequencies concentrating in the Fourier domain as spike/star-shaped peak areas [8] and so many frequency domain based filters are proposed. The filters in frequency domain include band reject filters, notch filters, Weiner filter, Ideal and Butterworth low-pass filters [9]. The band reject filter replaces specific circular symmetric frequency band around the direct current (DC) coefficient though the noisy frequencies are concentrated at fewer frequency positions of the band. Notch filters reject specific frequency region around a predefined central frequency from which Gaussian notch filters are widely used for periodic noise reduction due to its simplicity and compactness [9]. The performance of the Gaussian notch filter is limited to smaller quantum of noise strength due to its non-adaptive nature in fixing the size of filter window and other filter coefficients for various noise levels. It also rejects noisy peak positions without restoring them and so it failed to maintain fine image details. Ideal and Butterworth low-pass filters [10] irrespective of the corruptive status, allow only the central low-pass frequency areas around the DC coefficient defined by the predefined radius of the Fourier transformed image and rejects high frequencies outside the low-pass region.

Though spatial domain filters find difficulties in restoring periodic noise, there are many spatial filters in the literature [11–14]. However, these algorithms are not capable of removing high-density periodic noise since the noisy spectrum is distributed throughout the image in spatial domain. Addressing the limitations of spatial domain based filters, many adaptive Fourier transform-based algorithms are also reported in the literature [3, 6, 15–20]. Aizenberg and Butakoff [17] proposed an automated algorithm in frequency domain where a frequency is detected as noisy if the ratio of the frequency under concern and the median of frequencies defined by a static window exceeds a predefined threshold. The noisy peaks are then normalised by a static notch filter to attenuate detected noisy peak areas. However, its limitations in the form of un-optimised threshold parameter in detecting noisy peaks and static correction window motivated later research to come up with better results. The Fourier space median filter proposed by Hudhud and Turner [18] restores manually detected noisy peak areas by median of pixels from a static predefined neighbourhood. Jing and Liu [2] proposed a periodic noise reduction algorithm in bloodstain images using noisy peak identification and reduction stages, but the algorithm restores only the detected peak positions while leaving the associated noisy areas as such. Konstantinidis *et al.* [19] proposed a modified non-adaptive notch-based filters to restore images using static cross-shaped window. Ketenci and Gangal [20] introduced an adaptive star-shaped Gaussian notch filter for denoising periodic/quasi-periodic noise, but its performance is limited due to the filtering stage with a notch filter. Payman *et al.* [6] proposed a region growing-based algorithm to restore images corrupted by periodic noise. However, its performance is limited due to complex region growing operations in frequency domain. In addition, the algorithm also suffers most of the limitations of notch-based filters. The algorithms discussed in this section, though are good in meeting some requirements of periodic noise filtering, failed in simultaneously meeting other important aspects of image restoration such as computational efficiency, accurate identification

of noisy peak positions, restoration of noisy frequencies instead of rejection, maintaining fidelity in restored outputs [5] and so on.

This paper presents a windowed adaptive frequency domain-based switching minimum filter for the restoration of images corrupted with periodic noise by addressing the limitations of notch-based filters. Unlike other algorithms in the literature, the proposed filter highlights the noisy regions and effectively detects the noisy peak areas into noise map image by dividing the frequency domain image into four quadrants. The algorithm has the better ability to differentiate noisy frequencies from the uncorrupted ones since it separately identifies the noisy peak and its associated areas. This paper is organised into four sections. Section 2 details the proposed restoration filter. Experimental results and simulation analysis are made in Sections 3 and Section 4 concludes the paper.

2 WASMF algorithm

The proposed WASMF algorithm addresses the limitations of notch-based restoration algorithms and restores images corrupted with periodic noise. Initially, it highlights the noisy regions by convolving the origin shifted Fourier transformed corrupted image with Laplacian directional masks. The proposed peak detection algorithm then detects the noisy peaks from the directional image and generates the noise map image.

In the filtering stage of the algorithm, the adaptive switching minimum filter restores the detected noisy frequencies. Finally, inverse shifting and inverse Fourier transform operations reconstructs the restored image. If I is the input corrupted image of size $M \times N$, its origin shifted Fourier transformed frequency domain image, F is determined as

$$F(u, v) = \frac{1}{MN} \sum_{x=0}^{M-1} \sum_{y=0}^{N-1} (-1)^{x+y} I(x, y)\, \mathrm{e}^{-\mathrm{j}2\pi((ux/M)+(vy/N))} \quad (1)$$

Here $(-1)^{x+y}$ and j, are the shifting and imaginary components, respectively. The Fourier transformed Lena image from Fig. 1*a* is shown in Fig. 1*b*. The proposed filtering scheme incorporates noise map generation and noise cancellation schemes for effectively denoising periodic noise from corrupted input images and these schemes are explained in the following subsections.

2.1 Noise detection algorithm

In order to make the noisy peak detection process easy, the algorithm starts by convolving the Fourier transformed image F with Laplacian directional masks to highlight the noisy frequencies from the uncorrupted ones. These highlighted peak areas corresponding to noisy frequency regions, which are to be masked out by the filtering process are now isolated and they look star-shaped peaks in the directional image. In order to make the peak detection process faster, the algorithm divides the directional image to four equal quadrants. In order to speed up further, the algorithm makes use of the symmetric property of Fourier spectrum and it processes the noisy peak area detection to the first two quadrants. The noisy peak areas of other two quadrants are determined by the symmetric property of Fourier spectrum. The algorithm finds the maximum peak positions of the first two quadrants among which only the positions of the maximum peaks whose frequency values exceed a threshold function, T are recorded as noisy peaks. The noisy areas associated with these peak positions are recorded in the binary noise map image and are then avoided from the noise detection process of latter iterations to find new peaks. The iterations of the algorithm are carried out until the algorithm stops finding new noisy peak positions over the threshold function. The flowchart of the algorithm is shown in Fig. 2 and the peak detection algorithm is detailed through the following steps.

Step 1: The magnitude image P of Fourier transformed image F is determined to make the calculations in real number domain. This

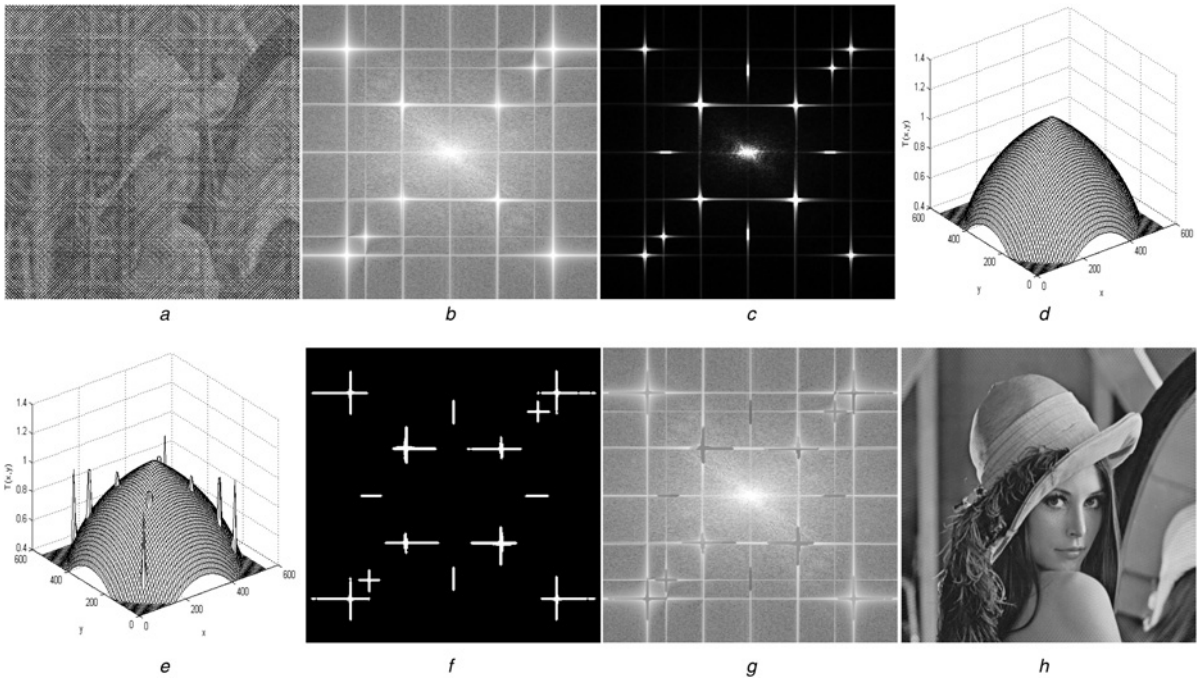

Fig. 1 *Different stages of WASMF*

a Corrupted image with $N_1 + N_2 + N_3$ type noise of strength $a = 0.5$
b Fourier transform of the corrupted image
c Normalised directional image
d Surface plot of threshold function when $c_2 = 1.1$
e Surface plot of normalised image when superimposed on threshold function
f Noise map image
g Restored Fourier transformed image
h Final restored image

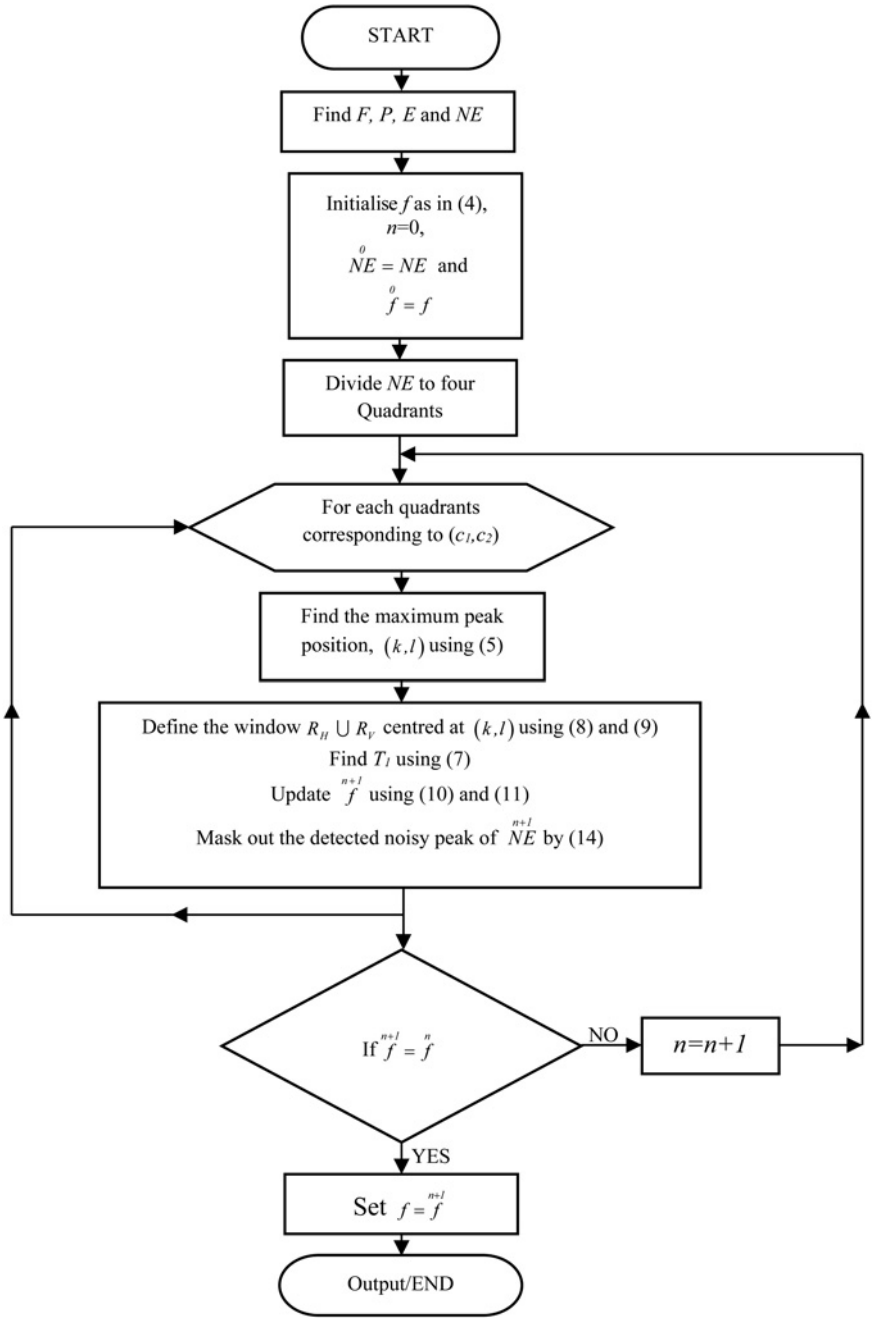

Fig. 2 *Flowchart of noise detection algorithm*

magnitude image P is then convolved with Laplacian directional masks to highlight the noisy frequency areas. The operation is defined by

$$E = \mathrm{Max}\left(\left|P \otimes w^k\right|\right), \quad k = 1 \text{ to } 4 \tag{2}$$

Here || stands for absolute value, $\otimes$ is the convolution operator, w^k is the kth Laplacian directional mask and

$$P(u, v) = \sqrt{R^2(u, v) + I^2(u, v)} \tag{3}$$

Here $R(u, v)$ and $I(u, v)$, respectively, are the real and imaginary components of $F(u, v)$. The Laplacian directional masks are shown in Fig. 3. The convolution operation of P with directional masks suppresses homogeneous uncorrupted frequencies and isolates the noisy peak positions of the magnitude image P. The directional image, E is then normalised to the interval [0 1] by dividing it with the maximum frequency value of E. In order to ease peak detection, threshold fixing and noise map generation processes, the contrast of this normalised directional image is increased by applying linear stretching [10] after saturating 1% of data in its lower and higher value ranges (2% in total). The *imadjust* function of Matlab performs the same. The algorithm uses the notation NE to represent the normalised and contrast stretched image. An example of NE image generated from Fig. 1*b* is shown in Fig. 1*c*. In the noise map generation scheme of the proposed algorithm, the corrupted frequency positions are identified into a binary noise map image, f of size $M \times N$. The algorithm sets $f(i_1, i_2)$ at position (i_1, i_2) to 1 when the frequency value, $NE(i_1, i_2)$ is corrupted and $f(i_1, i_2)$ to 0 when the frequency at $NE(i_1, i_2)$ is uncorrupted. Initially, the algorithm assumes that all frequencies of NE as uncorrupted and hence it resets all positions of binary noise map

w^1

-1	0	0	0	0
0	-1	0	0	0
0	0	4	0	0
0	0	0	-1	0
0	0	0	0	-1

w^2

0	0	-1	0	0
0	0	-1	0	0
0	0	4	0	0
0	0	-1	0	0
0	0	-1	0	0

w^3

0	0	0	0	-1
0	0	0	-1	0
0	0	4	0	0
0	-1	0	0	0
-1	0	0	0	0

w^4

0	0	0	0	0
0	0	0	0	0
-1	-1	4	-1	-1
0	0	0	0	0
0	0	0	0	0

Fig. 3 *Laplacian directional masks*

image, f to '0' as

$$f(i_1, i_2) = 0 \text{ for all } 0 \le i_1 \le M-1, \quad 0 \le i_2 \le N-1 \tag{4}$$

The iterative noise detection algorithm produces a sequence of directional and flag images in all iterations where NE^{n} and f^{n}, respectively, represent the directional and flag images in the nth iteration. Initially, iteration count n is set to zero indicating the 0th iteration. Also, the directional and flag images for the 0th iteration are, respectively, initialised as $\overset{0}{NE} = NE$ and $\overset{0}{f} = f$.

Step 2: In order to speed up the peak detection process, the directional image $\overset{0}{NE}$ is decomposed into four quadrants and each of these quadrants are processed individually. For the first two quadrants, the maximum frequency value $\overset{n}{NE}(k, l)$ in the normalised directional image $\overset{n}{NE}$ of the nth iteration is determined to check their corrupted status. Let (0, 0) and (0, 1) represent the values of (c_1, c_2) in the first and second quadrants, respectively. Since, the Fourier spectrum is symmetric to the opposite quadrants, the noisy peak areas corresponding to third and fourth quadrants are found from the results of second and first quadrants, respectively. In order to identify the noisy frequencies into the noise map image f, the algorithm performs following sub-steps to each quadrant defined by (c_1, c_2).

Step 2.1: The algorithm identifies the peak position (p, q) corresponding to the maximum frequency value of the quadrant (c_1, c_2) in (k, l) as

$$(k, l) = \underset{(p,q)}{\operatorname{argmax}} \left\{ \overset{n}{NE}(k, l): i_1 \le p \le i_1 + \frac{M}{2}, j_1 \le q \le j_1 + \frac{N}{2} \text{ and } \overset{n}{NE}(p, q) > T(p, q) \right\} \tag{5}$$

where

$$(i_1, j_1) \in \left\{ \left(\frac{c_1 \times M}{2}, \frac{c_2 \times N}{2} \right) \right\} \tag{6}$$

Here $(M/2, N/2)$ and (i_1, j_1), respectively, are the centre of the image and the starting position of each quadrant defined by (c_1, c_2). The decimal points of $(M/2, N/2)$ is truncated using flooring operation in the case of odd sized images.

Step 2.2: If $\overset{n}{NE}(k, l)$ is greater than or equal to the threshold function T, the algorithm assumes that the corresponding frequency peak at position (k, l) as corrupted. Figs. 1*d* and *e*, respectively, show the surface plots of threshold function, T and normalised image, NE when it is superimposed over threshold function, T. Once a peak frequency value at position (k, l) is detected as corrupted, the algorithm identifies the neighbouring noisy areas associated with $\overset{n}{NE}(k, l)$ in f^{n} by performing a thresholding operation. The algorithm considers all neighbouring frequencies of $\overset{n}{NE}(k, l)$ defined by $R_{\mathrm{H}} \cup R_{\mathrm{V}}$ over the threshold T_1 as corrupted. The threshold, T_1 used for deciding the noisy areas associated with the noisy peak at position (k, l) is determined as the mean of neighbouring frequencies of $\overset{n}{NE}(k, l)$ defined by the neighbourhood $R_{\mathrm{H}} \cup R_{\mathrm{V}}$. T_1 is mathematically expressed by

$$T_1 = \mathrm{Mean}\left(\left\{ NE_{i_1, i_2} : (i_1, i_2) \in R_{\mathrm{H}} \cup R_{\mathrm{V}} \right\} \right) \tag{7}$$

Here R_{H} and R_{V}, respectively, are the horizontal and vertical neighbourhood regions of interest centred at position (k, l)used for finding the noisy areas associated with $\overset{n}{NE}(k, l)$. R_{H} and R_{V} are, respectively, defined by

$$R_{\mathrm{H}} = \left\{ (k_1, k_2) : k - w_1 \le k_1 \le k + w_1, l - w_2 \le k_2 \le l + w_2 \right\} \tag{8}$$

$$R_{\mathrm{V}} = \left\{ (k_1, k_2) : k - w_2 \le k_1 \le k + w_2, l - w_1 \le k_2 \le l + w_1 \right\} \tag{9}$$

Here, w_1 and w_2, respectively, are the length and width parameters of the window $\mathrm{R_H} \cup \mathrm{R_V}$. The window area covered by $\mathrm{R_H} \cup \mathrm{R_V}$ when $w_1 = 1$ and $w_2 = 5$ is shown in Fig. 4. The algorithm uses cross-shaped neighbourhood $\mathrm{R_H} \cup \mathrm{R_V}$ to suit with star-shaped noisy peak areas.

Step 2.3: Once $\overset{n}{NE}(k, l) \ge T(k, l)$, the noisy region associated with $\overset{n}{NE}(k, l)$ is recorded in the noise map image, $\overset{n}{f}$ by applying a thresholding operation in the neighbourhood of $\overset{n}{NE}(k, l)$ defined

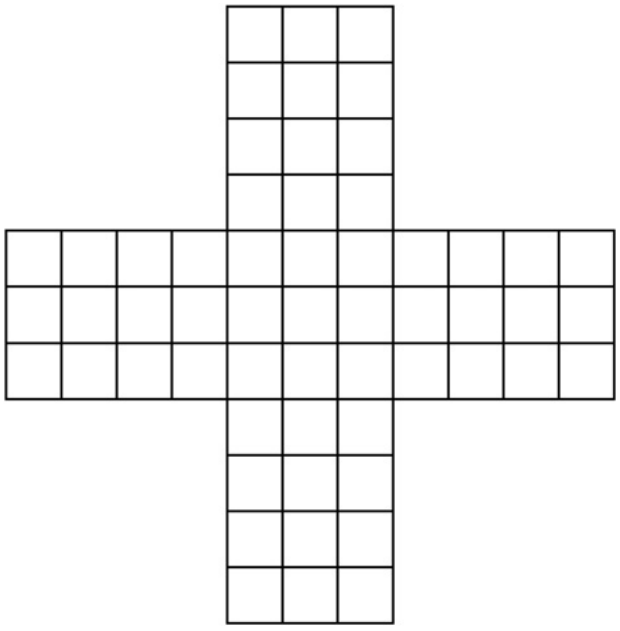

Fig. 4 *$R_H \cup R_V$ with $w_1 = 1$ and $w_2 = 5$*

by the neighbourhood $R_H \cup R_V$, i.e.

$$\overset{n+1}{f}(j_1, j_2) = \begin{cases} 1 \text{ if } \overset{n}{NE}(j_1, j_2) \geq T_1 \text{ and } (j_1, j_2) \in R_H \cup R_V \\ \overset{n}{f}(j_1, j_2) \quad \text{otherwise} \end{cases} \tag{10}$$

Once the flag image values corresponding to the quadrant (c_1, c_2) are determined, the algorithm updates the flag values corresponding to its symmetric quadrant in $\overset{n+1}{f}$ by determining the reflection operation. If (j_1', j_2') denotes the symmetric position of (j_1, j_2) corresponding to the opposite quadrant of (c_1, c_2), $\overset{n+1}{f}(j_1', j_2')$ is defined by

$$\overset{n+1}{f}(j'_1, j'_2) = \overset{n+1}{f}(j_1, j_2) \text{ for all } (j_1, j_2) \in R_H \cup R_V \tag{11}$$

where

$$j_1' = \begin{cases} M - j_1 + 1 \text{ if } M \text{ is even} \\ M - j_1 \quad \text{otherwise} \end{cases} \tag{12}$$

and

$$j_2' = \begin{cases} N - j_2 + 1 \text{ if } N \text{ is even} \\ N - j_2 \quad \text{otherwise} \end{cases} \tag{13}$$

This replacement of flag values of $\overset{n+1}{f}$ by utilising the symmetric properties of Fourier spectrum reduces the overall processing time of the noise detection scheme.

Step 2.4: Subsequently, to avoid the detected noisy areas from participating in subsequent iterations to find new noisy peak positions, the areas corresponding to the corrupted frequencies are diffused to zero in $\overset{n+1}{NE}$. Hence, the normalised directional image $\overset{n+1}{NE}$ of $n+1$ iteration becomes

$$\overset{n+1}{NE}(j_1, j_2) = \left\{ \begin{array}{l} 0 \text{ if } \overset{n+1}{f}(j_1, j_2) = 1 : (j_1, j_2) \in R_H \cup R_V \\ \overset{n}{NE}(j_1, j_2) \quad \text{otherwise} \end{array} \right\} \tag{14}$$

The algorithm is now continued from step 2.1 with next quadrant defined by (c_1, c_2).

Step 3: Once all noisy positions associated with detected noisy peaks from different quadrants of the current iteration are recorded in $\overset{n+1}{f}$, if $\overset{n+1}{f} \neq \overset{n}{f}$, it indicates that the current iteration has added new noisy positions to the flag image $\overset{n+1}{f}$. It necessitates another iteration to be performed for finding the undetected noisy areas and hence the iteration count, n is incremented by one and the next iteration is continued from step 2.

Step 4: If $\overset{n+1}{f} = \overset{n}{f}$, the algorithm stops the iterative noise detection process since the current iteration is not capable of finding new noisy positions and it fixes the final noise map image f as $f = \overset{n}{f}$.

The noise map image generated from Fig. 1*c* is shown in Fig. 1*f*. Since the algorithm individually identifies the noisy peaks and its associated noisy areas, it always has the better ability to differentiate noisy frequencies from the uncorrupted ones. In addition, the algorithm is faster since it processes noisy peak positions corresponding to the first two quadrants of *NE* in a single iteration.

2.2 Noise correction algorithm

The noise map image f generated by the noise detection stage provides the purity/corrupted status of each frequency in the frequency image F and this information is utilised by the noise correction scheme of the proposed algorithm to reconstruct the final restored image in frequency domain. For restoring corrupted frequencies in the Fourier transformed domain, the proposed algorithm uses a modified version of impulse correction scheme of one of our previously published works, the adaptive switching median filter (ASMF) [21]. ASMF is an adaptive filter designed for denoising salt and pepper impulses. Let Ω_i^W be the set of pixel positions in the neighbourhood $W \times W$ centred at position (i_1, i_2) defined by

$$\Omega^W(i_1, i_2) = \{(j_1, j_2): i_1 - k \leq j_1 \leq i_1 + k, i_2 - k \leq j_2 \leq i_2 + k\} \tag{15}$$

Here $k = (W-1)/2$ and W is the odd window size initialised to 3. The proposed noisy frequency correction algorithm replaces all noisy frequencies with the minimum of uncorrupted frequencies from the adaptively varying neighbourhood W × W. The algorithm is tracked through the following steps:

Step 1: If the binary noise map value $f(i_1, i_2)$ at position (i_1, i_2) corresponding to the frequency image value $F(i_1, i_2)$ is '0', it is maintained in the restored frequency image $\tilde{F}(i_1, i_2)$ since $F(i_1, i_2)$ is uncorrupted. Thus

$$\tilde{F}(i_1, i_2) = F(i_1, i_2) \tag{16}$$

Now the algorithm is continued from step 5.

Step 2: However, if the noise map value, $f(i_1, i_2)$ is '1', indicating $F(i_1, i_2)$ as corrupted, the algorithm collects the set of uncorrupted neighbouring frequency values of $F(i_1, i_2)$ defined by the window, $W \times W$ into the uncorrupted frequency set, ψ as

$$\psi = \{F(j_1, j_2): f(j_1, j_2) = 0 \text{ and } (j_1, j_2) \in \Omega^W(i_1, i_2)\} \tag{17}$$

Step 3: If the cardinality of ψ, N_ψ is found greater than 0, it is a good indication that sufficient number of uncorrupted frequencies are in the set ψ to replace corrupted frequency and the algorithm replaces the noisy frequency $F(i_1, i_2)$ with the minimum frequency of ψ as

$$\tilde{F}(i_1, i_2) = \text{Minimum}(\psi) \tag{18}$$

Step 4: Otherwise if $N_\psi = 0$, the window size W is adaptively increased to $W = W + 2$ for fetching uncorrupted frequencies and the process of replacing the corrupted $F(i_1, i_2)$ is continued from step 2 due to the absence of uncorrupted frequencies in ψ.

Step 5: The algorithm moves to next pixel position and the process of denoising is continued from step 1 until all frequency positions in F are processed. The final restored frequency image generated from Fig. 1*b* is shown in Fig. 1*g*.

Step 6: Once all the corrupted frequencies in F are replaced to generate the restored frequency domain image $\tilde{F}$, the algorithm performs the inverse of centre shifting and inverse Fourier transform to reconstruct the restored image, O as

$$O(x, y) = \sum_{u=0}^{M-1} \sum_{v=0}^{N-1} (-1)^{x+y} \tilde{F}(u, v)\, e^{j2\pi((ux/M)+(vy/N))} \tag{19}$$

The restored image produced by the proposed algorithm from Fig. 1*a* is shown in Fig. 1*h*.

Since the proposed algorithm incorporates distinct stages of noise detection and correction in frequency domain, it always has the better ability to restore corrupted images when compared to other algorithms. In addition, the adaptive nature of the restoration scheme to replace corrupted frequencies with the minimum of

IET Image Process., 2016, Vol. 10, Iss. 9, pp. 646–656

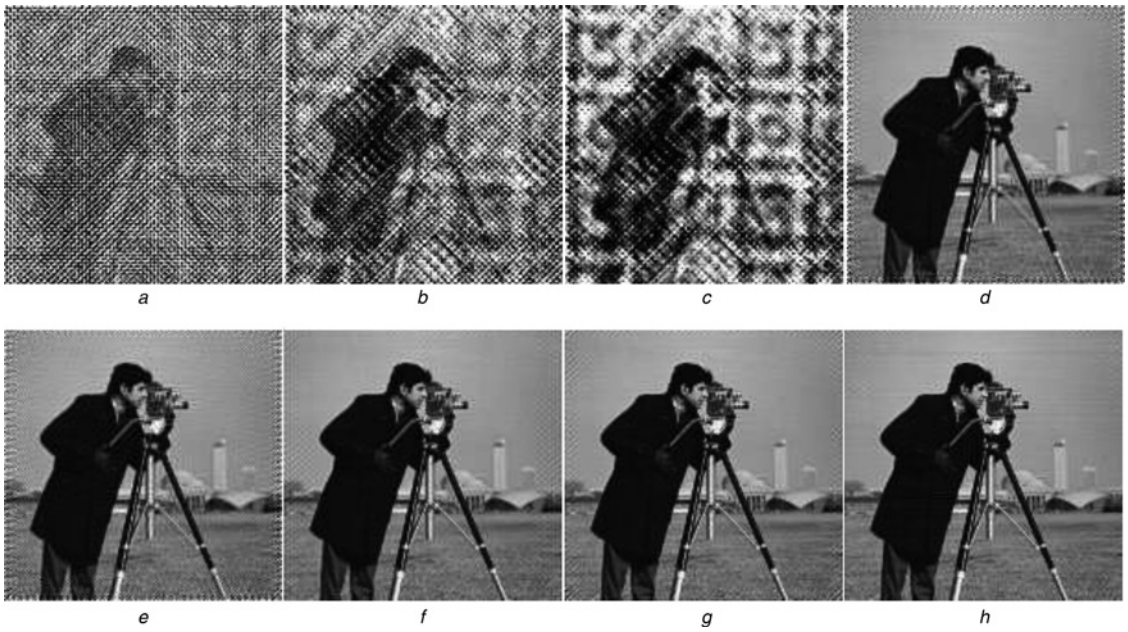

Fig. 5 *Outputs of algorithms in restoring the cameraman image corrupted with $N_1 + N_2 + N_3$ type noise of strength a = 1.0*

a Corrupted image
b SMF1
c SMF2
d GSSF
e WGNF
f AONF
g INRF
h WASMF

uncorrupted frequencies ensures that the restorer is uncorrupted and is from the nearest possible neighbourhood.

3 Experimental analysis and discussion

The performance of the proposed algorithm in restoring artificially corrupted digital images with periodic noise is tested with 15 8-bit standard images including cameraman, Lena, Barbara, boats, man, girl, house, baboon, pepper and so on of which the results from cameraman (256 × 256), Lena (512 × 512) and Barbara (512 × 512) images are presented in this paper for analysis. The proposed WASMF filter is compared with morphological filter (SMF1) [1], soft morphological filter (SMF2) [11], ideal low-pass filter (ILPF) [1], Aizenberg mean filter (AMF1) [16], Aizenberg median filter (AMF2) [15], Windowed Gaussian notch filter (WGNF) [17], Gaussian star-shaped filter (GSSF) [20], adaptive optimum notch filter (AONF) [6], interpolation notch reject filter (INRF) [19], Brickwall notch reject filter (BNRF) [19] and Gaussian notch reject filter (GNRF) [19] to show its improved performance. The algorithms are implemented using Matlab software installed in an Intel Core 2 Duo system with 4 GB RAM and 2.6 GHz clock rate.

The quantitative performance of the proposed algorithm is measured in terms of peak signal-to-noise ratio (PSNR), mean structural similarity index measure (MSSIM), percentage of not detected edges ξ_1, percentage of wrongly detected edges, ξ_2 and computational time (CT) in seconds. PSNR accounts the ratio of maximum signal strength to the power of noise that corrupts the signal. PSNR of the restored image O from the uncorrupted image U is defined by

$$\mathrm{PSNR} = 10\log_{10}\left(\frac{M\cdot N\cdot(255)^2}{\sum_{x=0}^{M-1}\sum_{y=0}^{N-1}\left|U(x,y)-O(x,y)\right|^2}\right)\mathrm{dB} \quad (20)$$

The visual quality of the restored images of different algorithms is assessed with mean structural similarity index measure (MSSIM), percentage of not detected edges ξ_1 and percentage of wrongly detected edges ξ_2. The formulation of MSSIM is as described in [22]. MSSIM provides a value in the interval [0 1] and is near to 1 when both the uncorrupted and the restored images are similar. ξ_1 is the percentage of absence of edge pixels in the restored image to the total edge pixels present in the noise-free image. Standard Canny algorithm [10] is used for performing the edge detection to determine ξ_1 and ξ_2. ξ_1 is defined by

$$\xi_1 = \left(\frac{\sum_{x=1}^{M}\sum_{y=1}^{N}N_{\xi_1}(x,y)}{\sum_{x=1}^{M}\sum_{y=1}^{N}A(x,y)}\right)\times 100\,(\%) \quad (21)$$

$$N_{\xi_1}(x,y) = \left\{\begin{matrix}1 \text{ if } A(x,y)=1 \text{ AND } B(x,y)=0\\ 0 \quad \text{otherwise}\end{matrix}\right\} \quad (22)$$

Here A and B, respectively, represents the edge images of original uncorrupted image, U and the restored image, O. ξ_2 is the percentage of absence of edge pixels in the noise-free image to the total edge pixels present in the restored image and is determined by

$$\xi_2 = \left(\frac{\sum_{x=1}^{M}\sum_{y=1}^{N}N_{\xi_2}(x,y)}{\left(MN-\sum_{x=1}^{M}\sum_{y=1}^{N}B(x,y)\right)}\right)\times 100\,(\%) \quad (23)$$

$$N_{\xi_2}(x,y) = \left\{\begin{matrix}1 \text{ if } A(x,y)=0 \text{ AND } B(x,y)=1\\ 0 \quad \text{otherwise}\end{matrix}\right\} \quad (24)$$

A good algorithm provides high PSNR and MSSIM values with less ξ_1 and ξ_2 values. Similar to other algorithms in the literature [6, 20], corrupted images are created by adding artificially generated sinusoidal noise patterns to the uncorrupted standard images. The

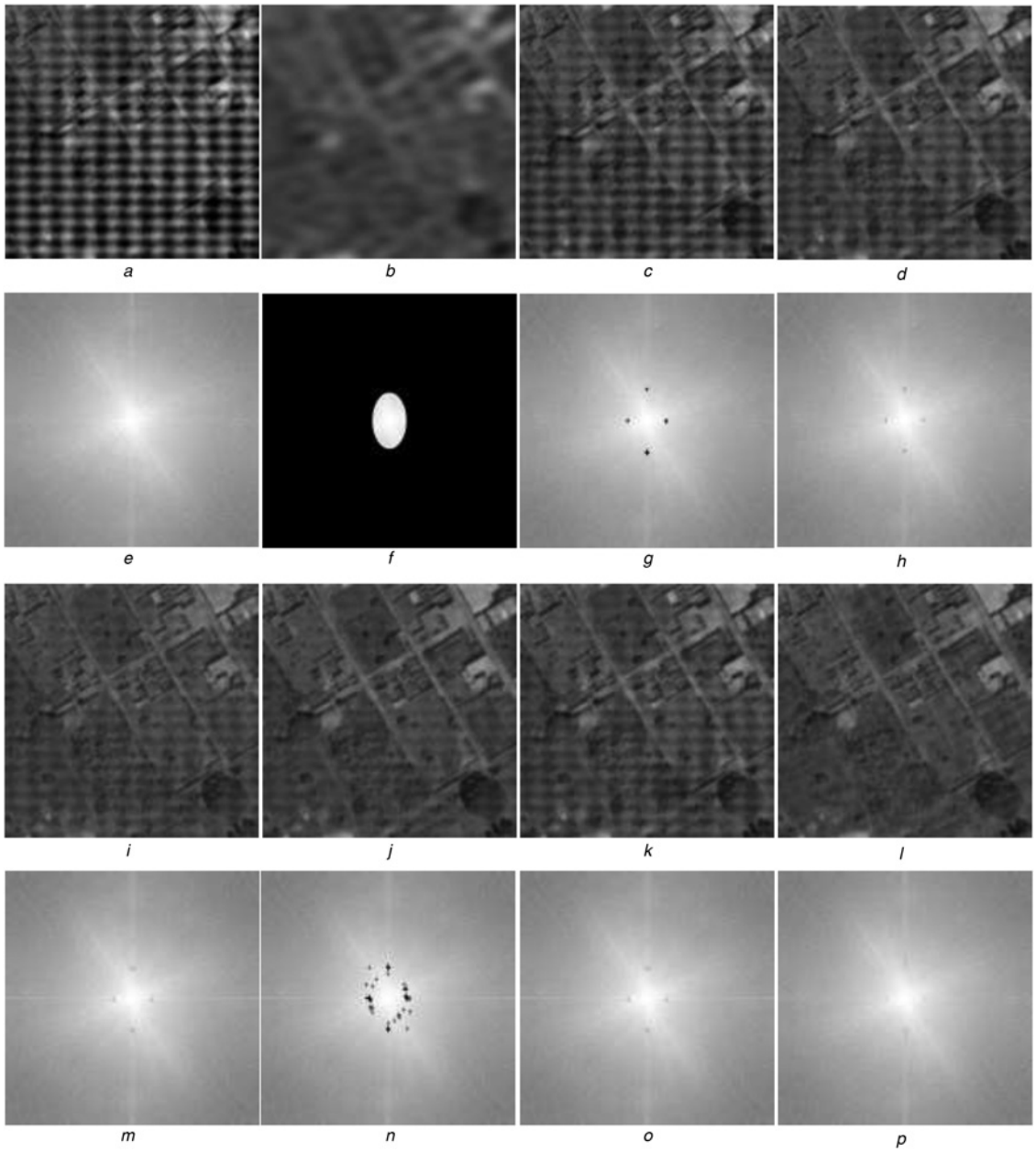

Fig. 6 *Outputs of algorithms in restoring the non-synthetic Ariel Pompeii image*

a Corrupted image
b Output of ILPF
c Output of GSSF
d Output of WGNF
e Fourier transform of the corrupted image
f Restored frequency domain image of ILPF
g Restored frequency domain image of GSSF
h Restored frequency domain image of WGNF
i Output of AONF
j Output of BNRF
k Output of GNRF
l Output of WASMF
m Restored frequency domain image of AONF
n Restored frequency domain image of BNRF
o Restored frequency domain image of GNRF
p Restored frequency domain image of WASMF

periodic noise models considered in this paper are

$$N_1(x, y) = a \times 255\big(\sin(x + y)\big) \tag{25}$$

$$N_2(x, y) = a \times 255\left(\begin{array}{l}\sin(8y) + \sin(8x) \\ + \sin\big(5.25x + 5.25y\big) + \sin\big(x + 5.25y\big)\end{array}\right) \tag{26}$$

$$N_3(x, y) = a \times 255\left(\begin{array}{l}\sin\big(1.8x + 1.8y\big) + \sin(x + y) \\ + \sin\big(2.2x + 2.2y\big) + \sin\big(1.8x - 1.8y\big) \\ + \sin(x - y) + \sin\big(2.2x - 2.2y\big)\end{array}\right) \tag{27}$$

Here a is the strength of the noise and $(x, y)$is the spatial

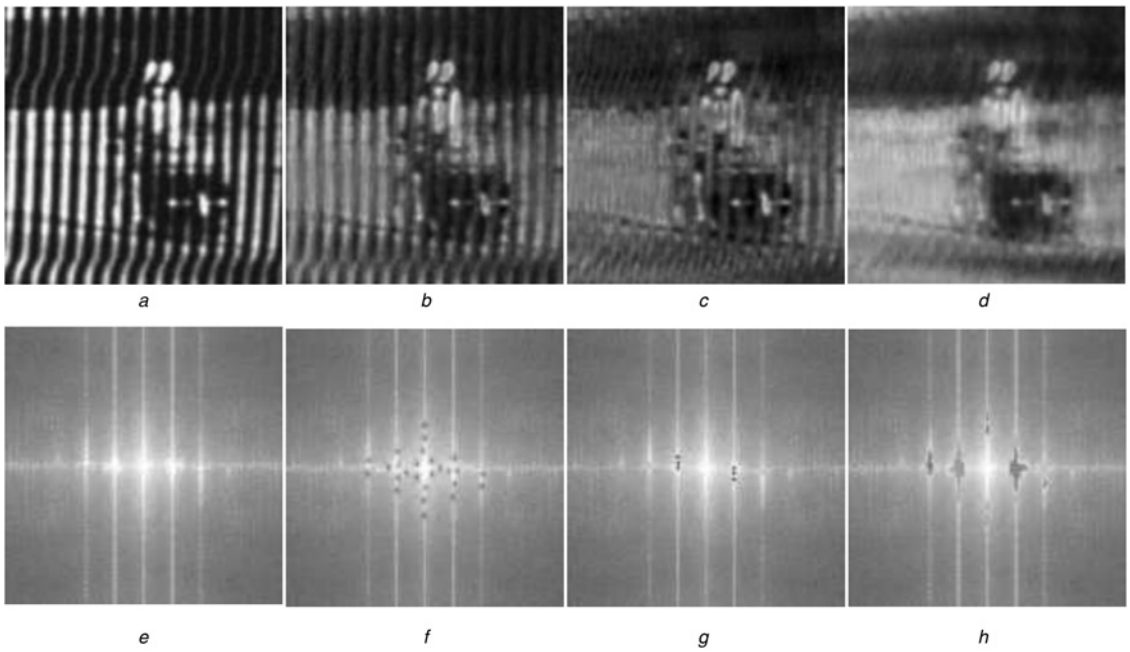

Fig. 7 *Outputs of algorithms in restoring the non-synthetic traffic image*

a Corrupted image
b Output of AONF
c Output of INRF
d Output of WASMF
e Fourier transform of the corrupted image
f Restored frequency domain image of AONF
g Restored frequency domain image of INRF
h Restored frequency domain image of WASMF

position. The performance of different algorithms in restoring non-synthetic images corrupted by periodic noise is tested with 15 different non-synthetic, naturally corrupted images. Fig. 5 shows the restored outputs of different algorithms while restoring cameraman image corrupted with $N_1 + N_2 + N_3$ type of periodic noise.

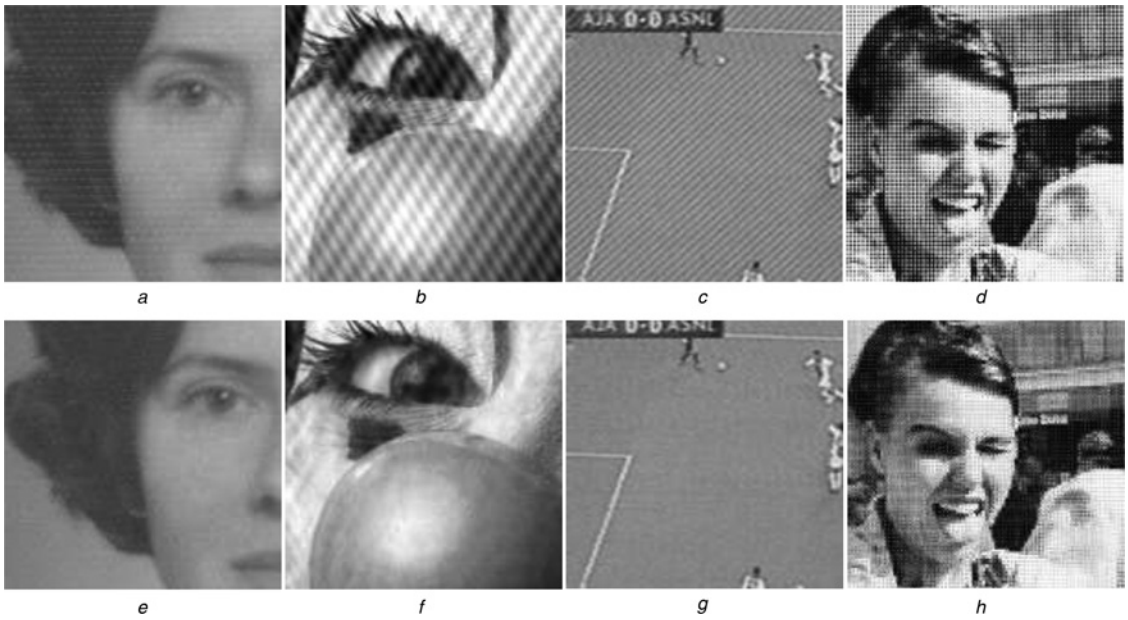

Fig. 8 *Outputs of WASMF in restoring non-synthetic images corrupted with periodic noise*

a Boy image
b Clown image
c Football match live video frame
d Lady image
e Restored boy image
f Restored clown image
g Restored football match live video frame
h Restored lady image

Figs. 6 and 7, respectively, show the restored outputs of different algorithms from non-synthetic, naturally corrupted Ariel Pompeii (1332 × 808) and traffic images (699 × 444). Fig. 8 shows the restored outputs of the proposed algorithm from non-synthetic boy (238 × 191), clown (294 × 294), football match video frame (367 × 291) and lady (1259 × 875) images. From Figs. 5–8, it is visible that the proposed WASMF algorithm is capable of producing better restored outputs when compared to other competing algorithms.

PSNR, MSSIM, $\xi_1 + \xi_2$ and CT produced by different algorithms while restoring cameraman, Lena and Barbara images corrupted with N_1, N_2 and N_3 noises for various noise strengths are tabulated in Tables 1–3. Table 4 shows the PSNR, MSSIM, $\xi_1 + \xi_2$ and the CT produced by different algorithms while restoring cameraman images corrupted with $N_1 + N_2 + N_3$ noises of equal strengths. Similar to other frequency domain-based comparative algorithms, the proposed algorithm also has a computational complexity of $O(n^2)$. Better quantitative values obtained by the proposed algorithm while restoring different images clearly indicate its improved performance over algorithm used in the comparative study.

3.1 Parameters and discussion

This subsection analyses the optimisation aspect of various parameters used by different algorithms in the comparative study. The performance of the standard and soft morphological filters depend on the structural element used for erosion and dilation operations. The performance of AMF1, AMF2, ILPF, WGNF, GSSF, AONF, INRF, BNRF and GNRF depends on low frequency areas that need to be avoided from noise detection and correction operations. AONF proposes a new method to identify the optimum low frequency region by partitioning the frequency image, F into non-overlapping arc shaped portions using concentric rings of 5-pixel width. However, this operation involves more calculations to identify the average of each arc portions and thereby increases the computational complexity of the algorithm.

Since AMF1, AMF2, ILPF, WGNF, GSSF, INRF, BNRF and GNRF used prefixed parameters for fixing the region of low frequency, AONF methodology is used for finding and fixing the low frequency region of all these algorithms. Also, these

Table 1 PSNR, MSSIM, $\xi_1 + \xi_2$ and CT analysis of different filters while restoring cameraman images corrupted with N_1 noise

Filters	Noise strength $a = 0.1$				Noise strength $a = 0.7$				Noise strength $a = 1.3$			
	PSNR	MSSIM	$\xi_1 + \xi_2$	CT	PSNR	MSSIM	$\xi_1 + \xi_2$	CT	PSNR	MSSIM	$\xi_1 + \xi_2$	CT
SMF1	23.22	0.70	44.46	0.82	21.01	0.62	83.15	0.86	19.45	0.53	99.11	0.87
SMF2	23.17	0.71	43.78	0.80	22.44	0.69	58.62	0.80	22.47	0.62	60.56	0.80
ILPF	24.74	0.78	42.41	0.93	23.41	0.73	49.31	1.16	21.21	0.67	55.35	1.22
AMF1	31.06	0.83	31.07	3.13	23.10	0.60	46.61	3.99	18.64	0.46	54.87	4.01
AMF2	33.83	0.90	17.80	5.70	21.40	0.58	49.69	5.76	16.35	0.41	59.86	5.84
WGNF	37.21	0.95	10.20	5.64	28.11	0.90	32.49	5.70	25.17	0.84	40.56	5.75
GSSF	38.93	0.96	8.27	0.98	20.93	0.87	45.77	1.13	17.14	0.80	41.34	1.73
AONF	42.62	0.97	5.17	0.75	32.84	0.89	20.42	1.68	28.04	0.81	30.77	2.13
INRF	42.79	0.98	6.46	2.27	36.50	0.90	15.66	2.54	31.40	0.82	27.62	3.02
BNRF	42.98	0.98	8.11	2.80	40.50	0.97	11.99	2.88	36.45	0.94	17.07	2.91
GNRF	44.15	0.99	7.22	2.33	41.90	0.97	8.69	3.06	39.26	0.94	11.40	4.98
WASMF	**45.02**	**0.99**	**4.73**	**2.64**	**43.23**	**0.98**	**6.88**	**2.97**	**40.92**	**0.97**	**9.57**	**3.14**

Table 2 PSNR, MSSIM, $\xi_1 + \xi_2$ and CT analysis of different filters while restoring Lena images corrupted with N_2noise

Filters	Noise strength $a = 0.1$				Noise strength $a = 0.7$				Noise strength $a = 1.3$			
	PSNR	MSSIM	$\xi_1 + \xi_2$	CT	PSNR	MSSIM	$\xi_1 + \xi_2$	CT	PSNR	MSSIM	$\xi_1 + \xi_2$	CT
SMF1	21.60	0.61	74.74	2.06	10.06	0.36	89.98	2.04	9.83	0.21	99.74	2.04
SMF2	25.12	0.72	71.71	2.24	12.10	0.48	87.23	2.23	10.86	0.32	98.70	2.24
ILPF	24.42	0.86	48.28	2.94	24.04	0.85	52.25	2.43	23.20	0.84	55.79	2.91
AMF1	33.07	0.95	20.93	5.04	17.66	0.61	36.39	5.72	12.37	0.43	82.44	6.71
AMF2	35.06	0.96	23.51	5.71	21.97	0.74	33.03	6.03	16.82	0.57	73.33	6.58
WGNF	37.01	0.96	12.16	6.76	24.84	0.91	36.19	7.66	20.01	0.82	45.81	9.63
GSSF	36.53	0.96	13.48	2.24	23.43	0.93	27.59	4.88	19.52	0.73	43.12	5.19
AONF	37.90	0.97	11.73	5.59	28.19	0.93	28.57	7.59	26.24	0.82	45.97	9.13
INRF	35.48	0.95	19.05	6.65	25.67	0.79	54.43	7.65	16.18	0.63	71.56	9.70
BNRF	36.27	0.95	15.56	5.27	26.91	0.87	48.32	5.72	22.61	0.75	67.12	7.12
GNRF	37.04	0.96	23.31	5.08	28.27	0.90	37.05	5.63	24.31	0.81	56.32	7.01
WASMF	**39.22**	**0.98**	**10.97**	**3.48**	**34.10**	**0.94**	**22.65**	**4.21**	**31.20**	**0.90**	**31.07**	**4.95**

Table 3 PSNR, MSSIM, $\xi_1 + \xi_2$ and CT analysis of different filters while restoring Barbara images corrupted with N_3 noise

Filters	Noise strength $a = 0.1$				Noise strength $a = 0.7$				Noise strength $a = 1.3$			
	PSNR	MSSIM	$\xi_1 + \xi_2$	CT	PSNR	MSSIM	$\xi_1 + \xi_2$	CT	PSNR	MSSIM	$\xi_1 + \xi_2$	CT
SMF1	22.09	0.54	78.49	2.28	12.63	0.27	98.63	2.33	9.01	0.10	99.29	2.10
SMF2	23.60	0.62	80.14	2.36	13.81	0.28	98.99	2.24	9.45	0.12	99.70	2.38
ILPF	31.08	0.96	40.35	3.14	26.27	0.92	47.75	2.56	22.00	0.88	54.42	3.04
AMF1	25.14	0.81	41.77	5.09	18.20	0.60	88.51	5.83	13.14	0.37	96.69	6.74
AMF2	29.03	0.89	32.64	5.92	18.99	0.65	75.39	6.26	14.65	0.39	88.91	6.60
WGNF	31.37	0.94	20.50	6.77	20.38	0.72	47.14	7.90	18.06	0.54	71.68	9.73
GSSF	31.38	0.95	16.53	2.32	19.34	0.81	35.68	4.94	17.65	0.68	47.51	5.38
AONF	36.13	0.96	10.55	5.60	24.82	0.86	27.23	7.74	21.70	0.72	41.02	9.20
INRF	36.06	0.94	13.00	6.68	24.47	0.60	25.45	7.78	19.25	0.42	43.54	9.82
BNRF	36.36	0.95	13.04	5.52	25.89	0.82	18.97	5.91	20.74	0.63	26.48	7.16
GNRF	38.17	0.97	12.16	5.29	31.42	0.87	14.76	5.84	26.69	0.76	19.49	7.16
WASMF	**41.03**	**0.99**	**7.92**	**3.26**	**34.43**	**0.97**	**13.52**	**4.18**	**30.16**	**0.93**	**17.16**	**4.73**

IET Image Process., 2016, Vol. 10, Iss. 9, pp. 646–656

Table 4 PSNR, MSSIM, $\xi_1 + \xi_2$ and CT analysis of different filters while restoring Cameraman images corrupted with $N_3 + N_3 + N_3$ noise

Filters	Noise strength $a = 0.1$				Noise strength $a = 0.7$				Noise strength $a = 1.3$			
	PSNR	MSSIM	$\xi_1 + \xi_2$	CT	PSNR	MSSIM	$\xi_1 + \xi_2$	CT	PSNR	MSSIM	$\xi_1 + \xi_2$	CT
SMF1	18.87	0.46	76.32	0.92	9.33	0.23	98.09	0.93	6.44	0.14	99.59	1.91
SMF2	19.81	0.43	82.87	1.02	10.77	0.27	96.88	1.31	6.72	0.19	98.90	2.12
ILPF	24.74	0.78	39.16	0.93	18.70	0.58	57.13	0.79	14.11	0.44	64.55	2.48
AMF1	22.82	0.58	39.03	2.88	14.61	0.26	67.56	3.99	9.51	0.19	77.39	5.40
AMF2	26.61	0.67	36.36	3.15	17.07	0.24	65.31	4.42	10.88	0.21	73.62	5.11
WGNF	27.63	0.86	23.38	3.43	18.23	0.44	58.38	5.46	13.68	0.29	66.23	7.51
GSSF	29.76	0.89	20.71	1.21	20.37	0.77	47.60	3.43	16.16	0.68	69.76	4.14
AONF	34.04	0.91	14.72	2.89	25.46	0.72	31.31	5.49	21.33	0.59	47.14	7.38
INRF	33.93	0.90	15.87	3.63	21.60	0.64	46.87	5.42	15.29	0.41	60.36	7.91
BNRF	34.61	0.92	17.79	2.85	22.16	0.52	43.82	4.16	16.91	0.35	57.50	5.56
GNRF	35.84	0.92	10.07	2.93	27.35	0.77	25.43	4.26	22.27	0.60	35.06	5.73
WASMF	**37.35**	**0.94**	**11.32**	**2.41**	**28.77**	**0.81**	**18.96**	**3.17**	**24.09**	**0.65**	**27.91**	**4.24**

Table 5 Average PSNR values obtained for $N_1 + N_2 + N_3$ noise by varying c_2 values

Noise strength, a	c_2				
	1	1.05	1.1	1.15	1.2
0.1	13.26	36.30	**37.72**	37.35	24.56
0.3	12.52	33.14	**33.69**	31.85	16.79
0.5	11.55	29.90	**30.88**	28.82	13.62
0.7	17.30	27.82	**28.86**	26.57	9.42
0.9	13.29	25.36	**27.05**	24.78	8.58

Table 6 Average PSNR values obtained for $N_1 + N_2 + N_3$ noise by varying W_1 and W_2 values

Noise strength, a	$W_1 = 1$		$W_1 = 2$		
	$W_2 = 2$	$W_2 = 3$	$W_2 = 2$	$W_2 = 3$	$W_2 = 4$
0.1	37.21	**37.72**	36.95	36.28	36.28
0.3	33.48	**33.69**	33.45	32.97	33.27
0.5	30.65	**30.88**	30.64	30.25	30.23
0.7	28.76	28.86	**28.94**	28.21	27.84
0.9	26.73	27.05	**27.30**	26.31	25.98

algorithms depend on the threshold value used for detecting noisy peak areas and the window size used for diffusing the noisy peak areas. Although these parameters vary according to the type of noise and images, the algorithms fix these parameters non-adaptively and it remains as the major drawback. INRF, BNRF and GNRF use static prefixed windows irrespective of noisy conditions to detect and mitigate noisy peak areas in the frequency domain. Moreover, INRF replaces detected corrupted frequency positions by the average of pixels determined from a prefixed neighbourhood. Since INRF considers both corrupted and uncorrupted frequencies while determining the average value to replace noisy peak areas, it generates much distortion in the restored outputs. All the other parameters of the algorithms used in the comparative study are fixed as suggested in the respective papers.

The performance of the proposed WASMF algorithm depends on the parameters, T, W_1 and W_2. Suitable values of these parameters are found out by testing the algorithm on different images with varying noise levels. From Fig. 1, it is obvious that the frequency values of frequency domain image F exponentially decrease from the centre position to the borders of the image. Hence, the threshold T should be a function of distance from the centre of the image since it is highly position dependant. Accordingly, T is formulated as

$$T(x, y) = \mathrm{Max}\left(c_1, c_2 \times \log_{10}\left(10 d_{x,y}\right)\right) \tag{28}$$

Here c_1 is the minimum tolerance level for being a noisy peak area and it is fixed to 0.4 after analysing different image cases. Also, $d_{x,y}$ is the normalised Euclidean distance of (x, y) from the centre of the image $(M/2, N/2)$.

In (25), $c_2 \times \log_{10}(10 d_{x,y})$ is a log transformation [23] and c_2 is a multiplicative parameter used for ensuring that the surface generated by the transformation is always above the uncorrupted version of the Fourier transformed image and it is fixed to 1.1 after conducting different experiments. Average PSNR values obtained from ten different images by varying noise strength of $N_1 + N_2 + N_3$ type noise are provided in Table 5. Fig. 1*d* shows the surface plot of T with $c_2 = 1.1$. Although the current formulation of T provides reasonable results, adaptive approaches that suit the image specific noisy conditions can be attempted as a future work to improve the performance of the proposed algorithm. The window parameters, W_1 and W_2 are used for covering the noisy areas associated with noisy peaks.

It is experimentally observed that the area covered by the window $R_H \cup R_V$ should be small enough when noise strength is very low. Also, when images are corrupted with higher quantum of periodic noise, it is obvious that the noisy areas that are not covered by the current iteration will be detected in the next iteration since the values corresponding to these areas are higher than the threshold T. By considering these facts, the values of W_1 and W_2 are, respectively, set to 1 and 5. $R_H \cup R_V$ with these parameters is shown in Fig. 4. Average PSNR values obtained from ten different images by varying noise strength of $N_1 + N_2 + N_3$ type noise for different values of W_1 and W_2 are provided in Table 6. In Table 1-6, the best experimental values obtained for all criteria used in the comparative study are highlighted by using bold face for easy reference.

4 Conclusion

This paper presented an adaptive frequency domain-based switching filter in frequency domain by incorporating distinct noise detection and correction stages for the restoration of digital images corrupted with periodic noise. The noisy frequency detection stage of the proposed scheme is incorporated with the peak detection and noise map generation algorithms to effectively identify the noisy peak areas into a binary flag image. The noise correction scheme restores the detected noisy peak areas of the input corrupted image with the mean of the nearest possible uncorrupted frequencies. Experimental results in terms of subjective and objective metrics showed that the performance of proposed filter in restoring periodic noise corrupted images is better when compared to other algorithms used in the comparative study.

5 References

1 Hansen, C.N.: 'Understanding active noise cancellation' (CRC Press, 2002)

2 Chen, X.L., Zhao, H.M., Li, P.X., *et al.*: 'Remote sensing image-based analysis of the relationship between urban heat island and land use/cover changes', *Remote Sens. Environ.*, 2006, **104**, (2), pp. 133–146

3 Jing, W., Liu, D.C.: '2-D FFT for Periodic Noise Removal on Strain Image'. Proc. Int. Conf. Bioinformatics and Biomedical Engineering, Chengdu, China, June 2010, pp. 1–4
4 Jackson, K.G., Townsend, G.B.: 'TV & video engineer's reference book' (Elsevier, 2014)
5 Atul, R.: 'An empirical study of periodic noise filtering in Fourier domain: an introduction to novel autonomous periodic noise removal algorithms' (LAMBERT Academic Publishing, 2013)
6 Payman, M., Masoumzadeh, M., Habibi, M.: 'A novel adaptive Gaussian restoration filter for reducing periodic noises in digital image', *Signal Image Video Process.*, 2013, **7**, (5), pp. 1–13
7 Feuerstein, D., Kim, H.P., Martyn, G.B.: 'Practical methods for noise removal: applications to spikes, nonstationary quasi-periodic noise, and baseline drift', *Anal. Chem.*, 2009, **81**, (12), pp. 4987–4994
8 Seguret, S.A.: 'Filtering periodic noise by using trigonometric kriging', in Matheron, G., Armstrong, M. (Eds.): 'Geostatistics' (Springer, Netherlands, 1989), pp. 481–491
9 Marques, O.: 'Practical image and video processing using MATLAB' (John Wiley & Sons, 2011)
10 Katsaggelos, A.K.: 'Digital image restoration' (Springer Publishing Company, 2012)
11 Zhen, J., Liao, H., Zhang, X., *et al.*: 'Simple and efficient soft morphological filter in periodic noise reduction'. Proc. IEEE TENCON, Hong Kong, China, November 2006, pp. 1–4
12 Zhen, J., Ming, Z., Li, Q., *et al.*: 'Reducing periodic noise using soft morphology filter', *J. Electron.*, 2004, **21**, (2), pp. 159–162
13 Ji, T.Y., Lu, Z., Wu, Q.H.: 'Optimal soft morphological filter for periodic noise removal using a particle swarm optimiser with passive congregation', *Signal Process.*, 2007, **87**, (11), pp. 2799–2809
14 Ji, T.Y., Lu, Z., Wu, Q.H.: 'A particle swarm optimizer applied to soft morphological filters for periodic noise reduction', *LNCS: Appl. Evolu. Comput.*, 2007, **4448**, pp. 367–374
15 Aizenberg, I., Butakoff, C.: 'Frequency domain median like filter for periodic and quasi-periodic noise removal'. Proc. SPIE 4667, Image Processing: Algorithms and Systems, San Jose, CA, January 2002, pp. 181–191
16 Aizenberg, I., Butakoff, I.: 'Nonlinear frequency domain filter for quasi periodic noise removal'. Proc. Int. TICSP Workshop on Spectra Methods and Multirate Signal Processing, 2002, pp. 147–153
17 Aizenberg, I., Butakoff, I.: 'A windowed Gaussian notch filter for quasi-periodic noise removal', *Image Vis. Comput.* 2008, **26**, (10), pp. 1347–1353
18 Hudhud, G.A., Turner, M.J.: 'Digital removal of power frequency artifacts using a Fourier space median filter', *Signal Process. Lett.*, 2005, **12**, (8), pp. 573–576
19 Konstantinidis, A.C., Olivo, A., Munro, P.R., *et al.*: 'Optical characterisation of a CMOS active pixel sensor using periodic noise reduction techniques', *Nuclear Instr. Methods Phys. Res. A, Accelerators Spectrometers Detectors Assoc. Equip.*, 2010, **620**, (2), pp. 549–556
20 Ketenci, S., Gangal, A.: 'Design of Gaussian star filter for reduction of periodic noise and quasi-periodic noise in gray level images'. Proc. Int. Conf. Innovations in Intelligent Systems and Applications, Trabzon, Turkey, July 2012, pp. 1–5
21 Nallaperumal, K., Varghese, J., Saudia, S., *et al.*: 'Salt & pepper impulse noise removal using adaptive switching median filter'. Proc. Int. Conf. IEEE OCEANS, Singapore, May 2007, pp. 1–8
22 Wang, Z., Bovik, A.C., Sheikh, H.R., *et al.*: 'Image quality assessment: from error measurement to structural similarity', *IEEE Trans. Image Process.*, 2004, **13**, (4), pp. 600–612
23 Sonka, M., Vaclav, H., Roger, B.: 'Image processing, analysis, and machine vision' (Cengage Learning, 2014)